Int J Theor Phys (2015) 54:4100–4109
DOI 10.1007/s10773-014-2481-2

Finite element Calculations of $\mathcal{PT}$-Symmetric Bose-Einstein Condensates

Daniel Haag · Dennis Dast · Holger Cartarius · Günter Wunner

Received: 30 October 2014 / Accepted: 16 December 2014 / Published online: 22 January 2015

Abstract $\mathcal{PT}$-symmetric systems have been intensively studied in optical waveguides, where the $\mathcal{PT}$ symmetry is achieved by pumping and absorption processes. In such systems the $\mathcal{PT}$ symmetry leads to a wide range of effects promising technical and scientific applications. By analogy, balanced gain and loss of particles in Bose-Einstein condensates (BEC) can be described by introducing a $\mathcal{PT}$-symmetric imaginary potential into the Gross-Pitaevskii equation (GPE). This equation can be solved numerically by various methods including the finite element approach. We apply this method to the GPE with arbitrary complex potentials and explicitly solve a double-well potential with shifted barriers.

Keywords Bose-Einstein condensation · Finite element method · $\mathcal{PT}$ symmetry

1 Introduction

An important part of studying systems of ultracold atoms is the consideration of particle exchange with the environment. Gain and loss of particles can be described in a many-particle picture by a Lindblad master equation [1]. However, these calculations are very time consuming. To treat complex systems as extended three-dimensional potentials an effective single-particle description is completely sufficient in the condensed phase. The derivation of a mean-field approximation leads to a Gross-Pitaevskii equation (GPE) with complex potentials [2–4]. Even though the GPE has limitations in describing the dynamics in the vicinity of instabilities, it provides very accurate stationary solutions for temperatures considerably smaller than the critical temperature for Bose-Einstein condensation [5, 6].

Imaginary potentials have already been successfully used to introduce particle exchange into the GPE. Negative imaginary potentials are employed to model dissipation from optical

D. Haag (✉) · D. Dast · H. Cartarius · G. Wunner
1. Institut für Theoretische Physik, Universität Stuttgart,
Pfaffenwaldring 57, 70550, Stuttgart, Germany
e-mail: daniel.haag@itp1.uni-stuttgart.de

lattices [7, 8] as well as particle losses due to inelastic three-body collisions [9, 10]. Furthermore the feeding of particles from a thermal cloud is described by positive imaginary potentials [10].

Since complex potentials render the Hamiltonian non-Hermitian, it is not guaranteed that true stationary states can be found. However, if the gain and loss contributions are chosen in such a way that the resulting system is $\mathcal{PT}$-symmetric, where $\mathcal{P}$ denotes the parity operator $\hat{x} \to -\hat{x}$, $\hat{p} \to -\hat{p}$ and $\mathcal{T}$ the time reversal operator $\hat{p} \to -\hat{p}$, $\mathrm{i} \to -\mathrm{i}$, the resulting Hamiltonian is at least pseudo-Hermitian [11–13]. It has been shown that such systems can exhibit entirely real eigenvalue spectra, therefore supporting stationary states [14–16].

On the one hand, much effort has been put into the formulation of a quantum theory that replaces the requirement of Hermiticity with the condition of pseudo-Hermiticity or $\mathcal{PT}$ symmetry. On the other hand these concepts have also been harnessed to develop a great variety of experimental accessible applications in optics and atomic physics [17–20]. Among these possible realizations the breakthrough succeeded in optical waveguide systems [17, 21–24], which are now one of the most active fields in experimental $\mathcal{PT}$ symmetry.

We are interested in employing these descriptions in the field of ultracold atoms. Until now no such system could be realized although suggestions exist. Double-well potentials are widely used to study effects of $\mathcal{PT}$-symmetric systems [25–29] and it has been shown that a BEC in such a potential with particle gain on one side and particle loss on the other can be an adequate candidate showing all effects known from linear $\mathcal{PT}$ symmetry while supporting a stable ground state [30–34]. The balanced influx and outflux of particles necessary to render the system $\mathcal{PT}$-symmetric can be achieved by embedding the double well into a Hermitian four-well potential [35] or transferring the particles from the loss to the gain well through a second $\mathcal{PT}$-symmetric condensate [36]. An alternative approach for coherent outcoupling of particles is the use of an focused electron beam [37] whereas the influx can be realized from a second condensate by trapping and releasing particles exploiting electronic excitations of the atoms [38].

These suggestions show possible first steps towards an experimental realization of a $\mathcal{PT}$-symmetric system. However, to fully utilize the pseudo-Hermitian description one has to apply it to potentials more complicated than a double well potential which can be well discussed even in a many-particle picture [4]. To achieve this we have to use methods going beyond the multi-mode models and the time-dependent variational principle used in the previous studies. We apply the finite element method with a basis of B-Splines to the dimensionless GPE with contact interaction,

$$\left[-\Delta + V(\mathbf{r}) + 8\pi N_0 a|\psi(\mathbf{r},t)|^2\right]\psi(\mathbf{r},t) = \mathrm{i}\frac{\partial}{\partial t}\psi(\mathbf{r},t), \tag{1}$$

where N_0 is the number of particles, a is the scattering length and $V(\mathbf{r})$ is a complex potential rendering the problem non-Hermitian. This method allows us to study arbitrary potentials with a precision only limited by the available computational resources.

In Section 2 we introduce the weak formulation of the GPE. The procedure is explained in detail to show the easy adaption to the non-Hermitian problem. The key differences to Hermitian problems will be shown and its numerical cost will shortly be discussed. In Section 3 we will then investigate a double-well potential motivated by our prior studies to test the method on a system well understood. By adding an asymmetric extension to the potential we demonstrate how this flexible method can add to the study of $\mathcal{PT}$-symmetric systems.

2 Weak Formulation

One way to achieve numerically accurate solutions for an arbitrary potential is to approximate the wave function by a finite dimensional basis. Since the wave functions for a continuous potential will be quite smooth, an ansatz of locally defined polynomials should yield reasonable solutions. We employ a basis of B-Splines which already has been very successfully used in the calculation of atomic spectra in strong magnetic fields [39].

We use de Boor's algorithm [40] where every spatial dimension is discretized by n_i vertices, constructing $n_i - 1$ elements in which the splines are used to interpolate the wave function. The B-Spline functions are defined recursively,

$$B_j^o(x) = \frac{x - s_j}{s_{j+o} - s_j} B_j^{o-1}(x) + \frac{s_{j+o+1} - x}{s_{j+o+1} - s_{j+1}} B_{j+1}^{o-1}(x), \tag{2}$$

$$B_j^0(x) = \begin{cases} 1, & \text{if } x \in [s_j, s_{j+1}) \\ 0, & \text{otherwise} \end{cases}, \tag{3}$$

where the s_j denote the spatial positions of the vertices and B_j^o denotes the B-Spline of oth order starting from the jth vertex. A B-Spline of oth order has a support of $n + 1$ adjacent elements. This algorithm only provides one spline in the first and last element respectively. To improve the quality of our basis in these elements, the first and last vertex are used $o + 1$ times when evaluating the formula (3). This leads to a basis with exactly $o + 1$ spline functions per element. This increases the dimension of our basis to $n_i - 1 + o$. An example of second order B-Splines over five vertices is shown in Fig. 1.

We assume that the wave functions vanish in the region outside the space covered by our grid. We take this boundary condition into account eliminating the outermost basis functions, thus reducing the dimension to a total of $d_i = n_i + o - 3$. The basis for higher dimensional systems is then created by a product ansatz of the one-dimensional basis functions. For three dimensions this reads $u_{j(n,m,l)}(x_0, x_1, x_2) = U_n(x_0)U_m(x_1)U_l(x_2)$. The full basis is then $D = d_0 d_1 d_2$ dimensional.

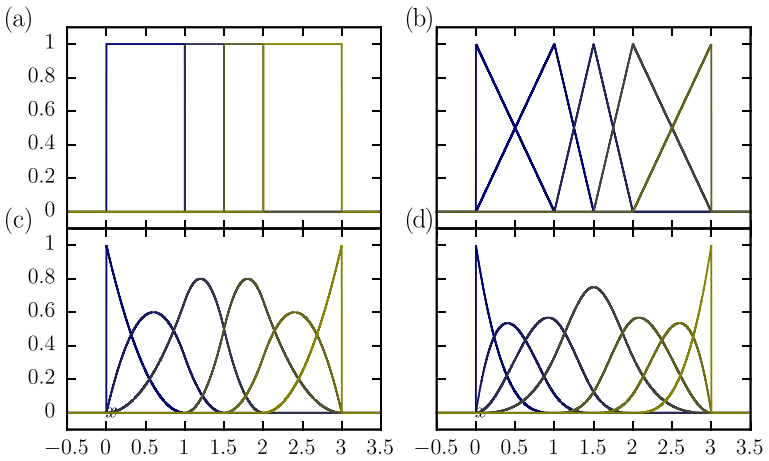

Fig. 1 A complete B-Spline basis for five vertices at $x = \{0, 1, 1.5, 2, 3\}$ of zeroth **a**, first **b**, second **c**, and third **d** order. The support of the B-Spline functions increases with increasing order leading to an increasing overlap between the functions. Only the first and the last functions contribute to the boundary value and thus are responsible for fulfilling the boundary conditions

Approximating the wave function by the expansion

$$\psi(\mathbf{r}) = \sum_{j=1}^{D} c_j u_j(\mathbf{r}) \tag{4}$$

generates the GPE in weak formulation,

$$\sum_{j=1}^{D} \left[\underbrace{\int \nabla u_j \nabla u_i + \left(V + 8\pi Na|\psi|^2\right) u_j u_i \, \mathrm{d}^n r}_{K_{ij}} \; c_j - \mu \underbrace{\int u_j u_i \, \mathrm{d}^n r}_{M_{ij}} \; c_j \right] = 0, \tag{5}$$

with the non-Hermitian matrix K describing the potential, the particle-particle interaction and kinetic contributions, and a mass matrix M describing the overlap of the non-orthogonal basis functions. In the linear case $Na = 0$, (5) can be reduced to the linear eigenvalue problem

$$K\mathbf{c} = \mu M\mathbf{c}, \tag{6}$$

which can be solved by various generalized eigenvalue solvers. It should be emphasized at this point that since the matrix is non-Hermitian, the eigenvalues will be complex in general.

For $Na \neq 0$ the K-matrix depends on the modulus squared of the wave function and thus on the B-spline coefficients c_j. Therefore a nonlinear system of equations has to be solved. In contrast to the generalized eigenvalue problem the solution of the system of nonlinear equations needs to be normalized,

$$\int |\psi|^2 \, \mathrm{d}^n r = c^\dagger M c = 1. \tag{7}$$

We can freely choose the global phase of the solution. While it would in principle be possible to use this freedom to reduce the dimension of the problem by setting $\mathrm{Im}\, c_j = 0$, this approach can lead to a ill-defined problem if the coefficient vanishes, $c_j = 0$. Therefore we use an arbitrary linear combination,

$$\sum_{j=1}^{D} b_j \mathrm{Im}\, c_j = 0, \tag{8}$$

with the weights b_j. Again the weights have to be chosen in such a way that the root search is well defined in most cases. We found randomly chosen weights to be very effective avoiding ill defined systems of equations. Please note that this is indeed only necessary for non-Hermitian problems. For any Hermitian system, μ would be a real number effectively reducing the number of unknown real parameters by one.

To solve the nonlinear system of equations we use derivative-based methods such as the Newton method, and to avoid time consuming numerical calculations, the required Jacobian is derived analytically. This gives rise to another complication: the modulus squared is not complex differentiable. However, this problem can be circumvented by rephrasing the D complex functions from (5) as $2D$ real functions. Additionally the D B-spline coefficients c_j and the chemical potential have to be split into real parameters. With the conditions given in (7) and (8) the nonlinear system of equations is $2D+2$-dimensional matching the number of parameters.

The parameter vector for the root search is now given by

$$\mathbf{a}^T = \left(\mathrm{Re}\mathbf{c}^T, \, \mathrm{Im}\, \mathbf{c}^T, \, \mathrm{Re}\mu, \, \mathrm{Im}\, \mu\right), \tag{9}$$

and the functions

$$\mathbf{f}(\mathbf{a}) = \begin{pmatrix} \text{Re}\,((K(\mathbf{c}) - \mu M)\mathbf{c}) \\ \text{Im}\,((K(\mathbf{c}) - \mu M)\mathbf{c}) \\ c^{T*} M c - 1 \\ \sum b_j \text{Im} c_j \end{pmatrix} \tag{10}$$

are differentiable with respect to each parameter.

Now the Jacobian $J_{ij} = \partial f_i / \partial a_j$ can be written in closed form,

$$J = \begin{pmatrix} S^{11} & S^{12} & -M\text{Re}\,\mathbf{c} & -M\text{Im}\,\mathbf{c} \\ S^{21} & S^{22} & -M\text{Im}\,\mathbf{c} & +M\text{Re}\,\mathbf{c} \\ 2(M\text{Re}\,\mathbf{c})^T & 2(M\text{Im}\,\mathbf{c})^T & 0 & 0 \\ \mathbf{0}^T & \mathbf{b}^T & 0 & 0 \end{pmatrix}, \tag{11}$$

with the $D \times D$-dimensional submatrices

$$S_{ij}^{11} = \text{Re}\,K + \text{Re}\,\mu M + \int 16\pi N a u_i u_j (\text{Re}\,\psi)^2 \mathrm{d}^n r, \tag{12}$$

$$S_{ij}^{12} = -\text{Im}\,K - \text{Im}\,\mu M + \int 16\pi N a u_i u_j \text{Re}\,\psi \text{Im}\,\psi\, \mathrm{d}^n r, \tag{13}$$

$$S_{ij}^{21} = \text{Im}\,K + \text{Im}\,\mu M + \int 16\pi N a u_i u_j \text{Re}\,\psi \text{Im}\,\psi\, \mathrm{d}^n r, \tag{14}$$

$$S_{ij}^{22} = \text{Re}\,K + \text{Re}\,\mu M + \int 16\pi N a u_i u_j (\text{Im}\,\psi)^2 \mathrm{d}^n r. \tag{15}$$

Since the matrices K and M are known from the evaluation of the functions $\mathbf{f}$, only the new integrals in the submatrices S have to be calculated to determine the Jacobian.

The non-Hermiticity of the problem provides only minor changes to the finite element method. First, since the chemical potential in general can be complex, the dimension of the problem increases by one. Second, it ensures that the wave functions can almost never be chosen real, instead each coefficient is complex consisting of a real and imaginary part. Altogether compared to the solution of the GPE with a real potential, the dimension of the problem increases by a factor of two.

3 Double Well Potential

We study the effects of deforming a double-well potential,

$$\begin{aligned} V(\mathbf{r}) = {} & 5\exp\left[-\frac{1}{2}x^2 - \frac{1}{10}\left(y^2 + z^2\right)\right] + \frac{1}{4}x^2 + z^2 + \begin{cases} y^2 & \text{if } y > 0 \\ (y+b)^2 & \text{if } y < -b \\ 0 & \text{else} \end{cases} \\ & + \mathrm{i}\gamma \exp\left[-\left(x + \sqrt{5}\right)^2 - y^2 - z^2\right] - \mathrm{i}\gamma \exp\left[-\left(x - \sqrt{5}\right)^2 - y^2 - z^2\right], \end{aligned} \tag{16}$$

where the deformation is controlled by the parameter b. Figure 2a shows the symmetric undeformed case $b = 0$ of a harmonic trap which is more elongated in x-direction than in the other two directions and separated into two wells by a Gaussian barrier. The imaginary part of the potential shown in Fig. 2c consists of two Gaussian functions positioned at the

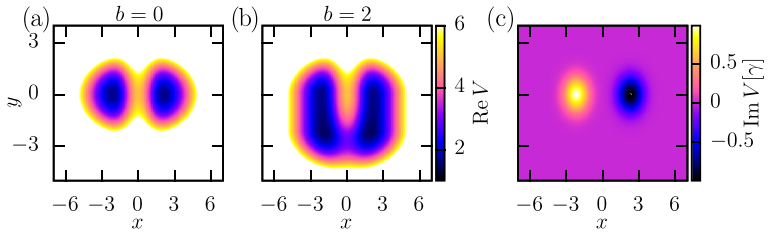

Fig. 2 **a** Real part of the symmetric double well with $b = 0$ and **b** the deformed double well for $b = 2$. Their common imaginary part is shown in **c**. For $b = 2$ an additional passage around the central barrier is created

minima of the double well. The left Gaussian is chosen positive, thus providing a gain of particles, while the right Gaussian is chosen negative, thus describing a loss of particles. The strength of the in- and outcoupling is described by the non-Hermiticity parameter γ. For a nonvanishing deformation $b > 0$ the center of the harmonic trap is shifted in y-direction from 0 to $-b$ and opens an additional passage for the particle transport between the two wells. This is shown in Fig. 2b for the special case $b = 2$. The passage should weaken the barrier and therefore increase the amount of particle in- and outcoupling for which $\mathcal{PT}$ symmetry can be observed. Note that all other numbers in the potential were fixed such that the results are comparable to those of double-well potentials in previous studies [34].

Figure 3 shows a comparison of the spectra of the original double well (a) and the deformed potential (b) for the linear system ($Na = 0$). Since the given linear problem can be separated into its three dimensions the excitation numbers in x-, y- and z-direction are used

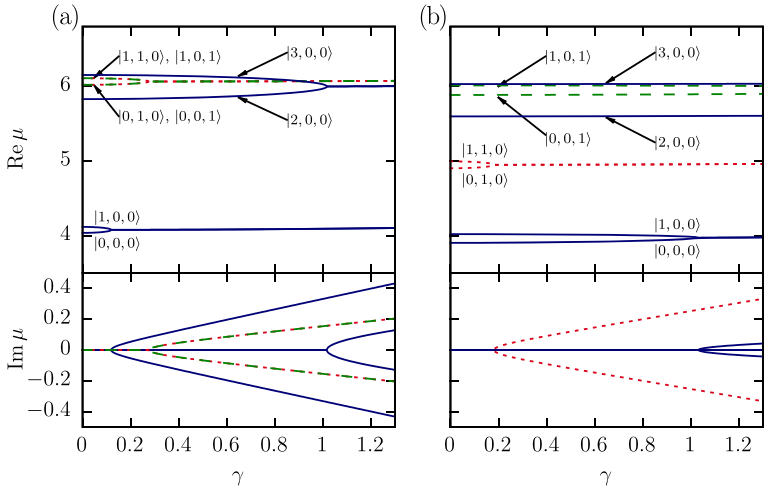

Fig. 3 Real and imaginary parts of the eigenvalues of the eight lowest lying states of the double-well potential **a** and the deformed potential **b** in the linear case as functions of the strength of the in- and outcoupling parameter γ. The branches are denominated using the excitation numbers in x-, y- and z-direction as quantum numbers, $|n_x, n_y, n_z\rangle$. The blue solid lines depict states with $n_y = n_z = 0$ while the red dotted (green dashed) lines depict states with $n_y = 1$ ($n_z = 1$). Every pair of states with consecutive excitations in x-direction but fixed quantum numbers n_y and n_z coalesces in an exceptional point, vanishes and gives birth to a set of two $\mathcal{PT}$-broken states. For the deformed potential all exceptional points with $n_y = 0$ are shifted to higher values of γ

as quantum numbers, characterizing the $\mathcal{PT}$-symmetric states $|n_x, n_y, n_z\rangle$. The blue solid lines including the ground and first excited state show the eigenvalues of the states without excitations in y- or z-directions, $|n_x, 0, 0\rangle$. The red dotted (green dashed) lines depict the eigenvalues of states which are excited in the y-(z-)direction, $|n_x, 1, 0\rangle$ ($|n_x, 0, 1\rangle$).

For a Hermitian system with $\gamma = 0$ all eigenstates are $\mathcal{PT}$-symmetric rendering the eigenvalues entirely real. For increasing parameters γ we find that the undeformed (Fig. 3a) system stays $\mathcal{PT}$-symmetric until the ground state and the first excited state coalesce and vanish in an exceptional point. Two $\mathcal{PT}$-broken states emerge at this point. As is always the case for $\mathcal{PT}$-symmetric systems their eigenvalues are related by a complex conjugation. This behavior is reproduced by all consecutive pairs of x-excitations within a manifold defined by a fixed y- and z-quantum number, $|0, n_y, n_z\rangle$ and $|1, n_y, n_z\rangle$. This behavior has already been studied extensively in the case of the ground and first excited state [26, 32–34].

For the deformed potential (Fig. 3b) the situation changes drastically. Most states confirm the assumption that the system should support higher currents in the $\mathcal{PT}$-symmetric phase. The exceptional points of all states with no excitations in y-direction, $n_y = 0$, are shifted to higher values of γ. By contrast, the remaining two states with $n_y = 1$ shown in Fig. 3 coalesce at a slightly lower value of γ. For the overall system this means that the $\mathcal{PT}$ symmetry breaks at nearly the same value as before. This time however, the cause is not the bifurcation of the pair with the lowest energies but instead the bifurcation of the states excited in y-direction.

We want to emphasize that even if the ground state still exists and has a purely real energy it is no longer experimentally realizable in the linear system at the moment the $\mathcal{PT}$ symmetry gets broken. Every small deformation will lead to a contribution of the $\mathcal{PT}$-broken states, which will result in an infinite growth of the probability amplitude due to the state with $\mathrm{Im}\ \mu > 0$.

Although we introduced a new passage connecting the two wells and weakening the barrier, the system still cannot support a stronger current in the $\mathcal{PT}$-symmetric phase. To fully understand this effect, the wave functions of the states excited in y-direction are studied in detail. Figure 4 shows the states $|0, 1, 0\rangle$ (upper two panels) and $|1, 1, 0\rangle$ (lower two panels) for the double-well potential (left panel) and the deformed potential (right panel). The probability density is given in the form of an absorption image while the current density is depicted by arrows.

In the double-well case (Fig. 4 left panel) both states show a nodal line in y-direction. With additional views of the wave functions we checked that both wave functions are symmetric in z-direction. The energetically lower lying state with $n_x = 0$ (Fig. 4a) has a finite probability at the $x = 0$ plane. The second state with $n_y = 1$ (Fig. 4c) has an additional node at $x = 0$. The probability current density exhibits a strong flow of particles from the left to the right well. The highest fraction of these currents is present at the maxima of the particle density in y-direction.

When the barrier in y-direction is shifted and the potential is no longer symmetric with respect to the x-z-plane the two states become asymmetric as well. Both the symmetric (Fig. 4b) and the antisymmetric state in x-direction (Fig. 4d) follow the shift of the barrier. This places one of the two maxima in y-direction at $y = 0$ near the center of the original double well. This maximum becomes much stronger while the other one is damped indicating that the particles are accumulating at $y = 0$ for stronger a deformation. At this position the imaginary part of the potential is much higher leading to a stronger in- and outcoupling of particles. Due to the node in y-direction there is no significant current from the upper to the lower maxima. Therefore the main current from the left to the right well leads over the top of the potential barrier in x-direction. This behavior is similar

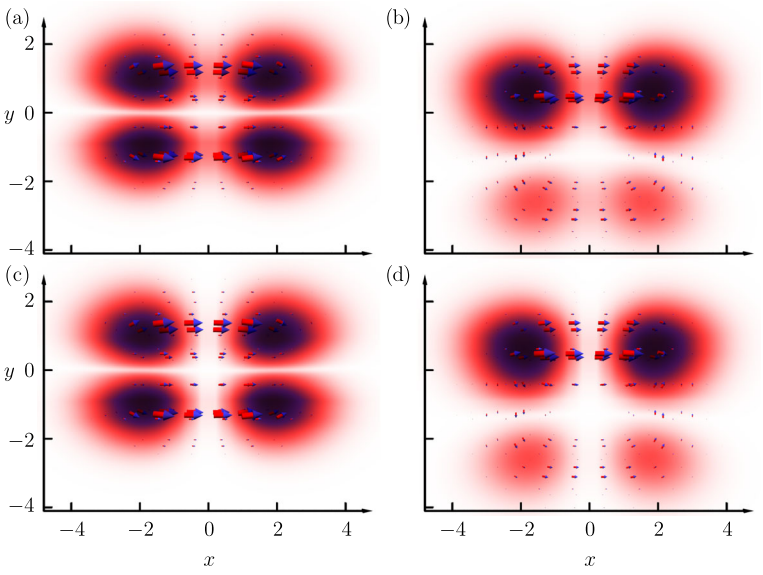

Fig. 4 View onto the $x-y$-plane of the double-well potential without (**a**),(**c**) and with (**b**),(**d**) a shift of the barrier. Particle density (darkened red and blue areas) and current density (red arrows with blue heads) of the first two antisymmetric states in y and symmetric states in z-direction for $\gamma = 0.1$. The states are symmetric (**a**),(**b**) and antisymmetric (**c**),(**d**) in x-direction respectively. In the symmetric double well ($b = 0$) the particles are symmetrically distributed between the two maxima in y-direction while in the shifted case ($b \neq 0$) most particles remain near $y = 0$

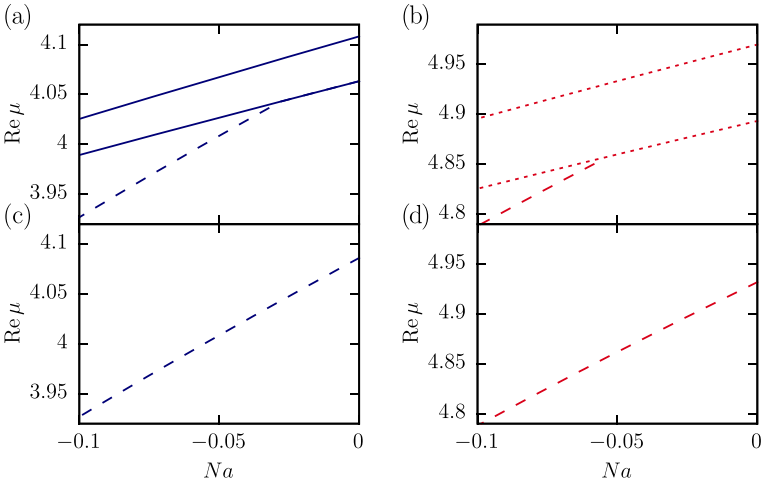

Fig. 5 **a** Real part of the chemical potential of the ground and first excited states of the double-well potential for $\gamma = 0.1$ for varying interaction strength. **c** For $Na \lesssim -0.03$ two $\mathcal{P}$-broken states (dashed lines) emerge from the ground state. For $\gamma = 0.2$ the $\mathcal{P}\widetilde{\mathcal{T}}$-symmetric states vanish and only the broken states remain. The two excited states with $n_y = 1$ of the double well with shifted barrier for $\gamma = 0.1$ (**b**) and $\gamma = 0.2$ (**d**) show the same behavior as the ground and first excited state in (**a**) and (**c**)

to that of the double well's ground state, where we have one maximum in each of the wells.

Since the excited states in y-direction become similar to the ground and first excited state of the symmetric double well $b = 0$, it is reasonable to compare these two sets of states also in the case of a nonvanishing particle-particle interaction. This comparison is done in Fig. 5, where the left panels show the ground and first excited state of the original potential ($n_z = n_y = 0$) and the right panels show the y-excited states ($n_y = 1$) for the shifted potential $b = 2$. We see immediately that both states behave similarly when the interaction strength is varied. The upper two panels (Fig. 5a, b) show the case $\gamma = 0.1$ well before the symmetry breaking. For an decreasing scattering length a the interaction grows stronger, leading to a separation of the two $\mathcal{PT}$-broken states from the energetically lower states even though the gain and loss of particles in the system is still low enough to support $\mathcal{PT}$-symmetric states. For parameters γ well beyond the exceptional point (Figs. 5c, d) only the corresponding $\mathcal{PT}$-broken states exist for all scattering lengths shown.

4 Conclusion

We have demonstrated that the concepts of FEM simulations can easily be applied to the non-Hermitian case of $\mathcal{PT}$-symmetric potentials. With an appropriate basis the problem is reduced to local integrations and a nonlinear root search which can be solved numerically using Newton methods. The Jacobian matrix was derived analytically for the nonlinear problem and can be computed numerically in a cheap way.

The method has been tested on a double well with a shifted barrier in y-direction creating an additional passage for the atom flow between the two wells. We showed that this enhances the range for which the ground state is $\mathcal{PT}$ symmetric. However, excitations in y-direction inhibit a current through the additional channel, leading to a symmetry breaking of the whole system. For the strongly shifted barrier discussed in this paper these excited states become very asymmetric and the repressed current in y-direction leads to a behavior of these states similar to the ground state of the original symmetric two well system.

References

1. Breuer, H.P., Petruccione, F.: The Theory of Open Quantum Systems, 1st edn. Oxford University Press, Oxford (2002)
2. Trimborn, F., Witthaut, D., Wimberger, S.: J. Phys. B **41**(17), 171001 (2008)
3. Witthaut, D., Trimborn, F., Hennig, H., Kordas, G., Geisel, T., Wimberger, S.: Phys. Rev. A **83**, 063608 (2011)
4. Dast, D., Haag, D., Cartarius, H., Wunner, G.: Phys. Rev. A **90**, 052120 (2014)
5. Anglin, J.R., Vardi, A.: Phys. Rev. A **64**, 013605 (2001)
6. Vardi, A., Anglin, J.R.: Phys. Rev. Lett **86**, 568 (2001)
7. Abdullaev, F.K., Konotop, V.V., Salerno, M., Yulin, A.V.: Phys. Rev. E **82**, 056606 (2010)
8. Bludov, Y.V., Konotop, V.V.: Phys. Rev. A **81**, 013625 (2010)
9. Moiseyev, N.: Non-Hermitian Quantum Mechanics. Cambridge University Press, Cambridge (2011)
10. Kagan, Y., Muryshev, A.E., Shlyapnikov, G.V.: Phys. Rev. Lett **81**, 933 (1998)
11. Mostafazadeh, A.: J. Math. Phys **43**, 205 (2002)
12. Mostafazadeh, A.: J. Math. Phys. **43**, 2814 (2002)
13. Mostafazadeh, A.: J. Math. Phys. **43**, 3944 (2002)
14. Bender, C.M., Boettcher, S.: Phys. Rev. Lett. **80**, 5243 (1998)
15. Bender, C.M., Boettcher, S., Meisinger, P.N.: J. Math. Phys. **40**, 2201 (1999)
16. Bender, C.M.: Rep. Prog. Phys. **70**, 947 (2007)

17. Klaiman, S., Günther, U., Moiseyev, N.: Phys. Rev. Lett. **101**, 080402 (2008)
18. Schindler, J., Li, A., Zheng, M.C., Ellis, F.M., Kottos, T.: Phys. Rev. A **84**, 040101 (2011)
19. Bittner, S., Dietz, B., Günther, U., Harney, H.L., Miski-Oglu, M., Richter, A., Schäfer, F.: Phys. Rev. Lett. **108**, 02410 (2012)
20. Mayteevarunyoo, T., Malomed, B.A., Reoksabutr, A.: Phys. Rev. E **88**, 022919 (2013)
21. Rüter, C.E., Makris, K.G., El-Ganainy, R., Christodoulides, D.N., Segev, M., Kip, D.: Nat. Phys. **6**, 192 (2010)
22. Guo, A., Salamo, G.J., Duchesne, D., Morandotti, R., Volatier-Ravat, M., Aimez, V., Siviloglou, G.A., Christodoulides, D.N.: Phys. Rev. Lett. **103**, 093902 (2009)
23. Peng, B., Özdemir, .K., Rotter, S., Yilmaz, H., Liertzer, M., Monifi, F., Bender, C.M., Nori, F., Yang, L.: Science **346**, 328 (2014)
24. Peng, B., Özdemir, Ş.K., Lei, F., Monifi, F., Gianfreda, M., Long, G.L., Fan, S., Nori, F., Bender, C.M., Yang, L.: Nat. Phys. **10**, 394 (2014)
25. Jones, H.F.: Phys. Rev. D **78**, 065032 (2008)
26. Cartarius, H., Haag, D., Dast, D., Wunner, G.: J. Phys. A **45**, 444008 (2012)
27. Cartarius, H., Wunner, G.: Phys. Rev. A **86**, 013612 (2012)
28. Konotop, V.V., Zezyulin, D.A.: Opt. Lett. **39**(5), 1223 (2014)
29. Midya, B.: Nonlinear Dyn. (2014). doi:10.1007/s11071-014-1674-9
30. Graefe, E.M.: J. Phys. A **45**, 444015 (2012)
31. Dast, D., Haag, D., Cartarius, H., Wunner, G., Eichler, R., Main, J.: Fortschr. Physik **61**, 124 (2013)
32. Rodrigues, A.S., Li, K., Achilleos, V., Kevrekidis, P.G., Frantzeskakis, D.J., Bender, C.M.: Rom. Rep. Phys. **65**, 5 (2013)
33. Dast, D., Haag, D., Cartarius, H., Main, J., Wunner, G.: J. Phys. A **46**, 375301 (2013)
34. Haag, D., Dast, D., Löhle, A., Cartarius, H., Main, J., Wunner, G.: Phys. Rev. A **89**, 023601 (2014)
35. Kreibich, M., Main, J., Cartarius, H., Wunner, G.: Phys. Rev. A **87**(R), 051601 (2013)
36. Single, F., Cartarius, H., Wunner, G., Main, J.: Phys. Rev. A **90**, 042123 (2014)
37. Gericke, T., Wurtz, P., Reitz, D., Langen, T., Ott, H.: Nat. Phys. **4**, 949 (2008)
38. Robins, N.P., Figl, C., Jeppesen, M., Dennis, G.R., Close, J.D.: Nat. Phys. **4**, 731 (2008)
39. Schimeczek, C., Wunner, G.: Comp. Phys. Comm. **185**(2), 614 (2014)
40. de Boor, C.: SIAM J. Numer. Anal. **14**(3), 441 (1977)